HCMP Characteristics Assessment for *in situ* Microenvironmental Force Measurement

By

Marta Rodríguez Navas

Biomedical Engineering BS, Polytechnic University of Madrid, 2022

Thesis

Submitted in partial fulfillment of the requirements for the Degree of Master of Science in the Graduate Program of Biomedical Engineering at Brown University

PROVIDENCE, RHODE ISLAND

MAY 2024

AUTHORIZATION TO LEND AND REPRODUCE THE THESIS

As the sole author of this thesis, I authorize Brown University to lend it to other institutions for the purpose of scholarly research.

Date 04/29/2024 Marta Rodriguez Navas

Marta Rodríguez Navas, Author

I further authorize Brown University to reproduce this thesis by photocopying or other means, in total or in part, at the request of other institutions or individuals for the purpose of scholarly research.

Date 04/24/2024 Marta Rodriguez Navas

Marta Rodríguez Navas, Author

This thesis by Marta Rodríguez Navas is accepted in its present form by the Center for Biotechnology as satisfying the thesis requirements for the degree of Master of Science

Date_____ Signature: _____

Dr. Eric M Darling, Advisor

Date_____ Signature: _____

Dr. Jeffrey Morgan, Reader

Date_____ Signature: _____

Dr. Haneesh Kesari, Reader

Approved by the Graduate Council

Date_____ Signature: _____

Dr. Andrew G. Campbell, Dean of the Graduate School

Table of Contents

Table of Figures

Table of Tables

Abstract of HCMP Characteristics Assessment for in situ Microenvironmental Force Measurement, by Marta Rodríguez Navas, ScM, Brown University, May, 2024.

Early tissue formation and regeneration is regulated by mechanical forces. However, few tools exist that can measure such forces *in situ* in cell-dense structures and in 3D. Measuring the deformation of embedded HCMP in microtissues can be used to address this gap in knowledge, but there is a lack of characterization for this approach. In this study, we compared HCMP with different sizes, which we hypothesized would measure different force ranges; stiffnesses which we hypothesized would impact measurement resolution; and protein coatings, to measure the forces in cell-cell and cell-ECM interactions. We also evaluated the accuracy of our methodology by modifying the undeformed size of the analyzed particles, treating our cells with cytoskeletal disruptors and comparing the use of a virtual Time 0 image with the real Time 0 images. We concluded that large soft probes provide the most accurate measurements and that protein-coated particles measure tensile forces while uncoated probes measure more compressive forces.

Chapter 1: Introduction

Mechanical signals and mechanotransduction play a key role during early tissue development, not only because they control the differentiation and proliferation of stems cells, [1,2], but also because different stem cell species have different stiffnesses, which means that they exert and sense mechanical forces of different ranges [3,4]; for example, human cortical neurons, lung epithelial cells and erythrocytes and have an elastic modulus in the range of 100 Pa, [3,5-8] while human breast and prostate cells have an elastic modulus on the 2000 Pa range [3,7,9]. For this reason, in early development and organogenesis, control stem cell fate (including differentiation and self- renewal) and can be exploited to promote regeneration and new tissue formation [2].

The mechanical properties of each cell, including their stiffness, are mainly given by the combination of their cytoskeleton and membrane [10]. The main components of the cytoskeleton are actin filaments, intermediate filaments, and microtubules [10]. These then adhere to proteins (receptors) in the cellular membrane to form junctions with the extracellular matrix (ECM) or other cells. An example of these would be adherens junctions, in which actin filaments are bound to cadherins located in the membrane which then are linked with other cadherins in the membrane of neighbor cells, or integrins which bind cells to their ECM and actin (Figure 1). Cell-ECM bindings are usually driven by an integrin that binds to collagen (Figure 1), and then transmits the force to the cytoskeleton which would then be transmitted to the nucleus which modulates the cell shape, differentiation, tissue formation, and development [11]. These bindings generate forces between cells and between the cell and ECM.

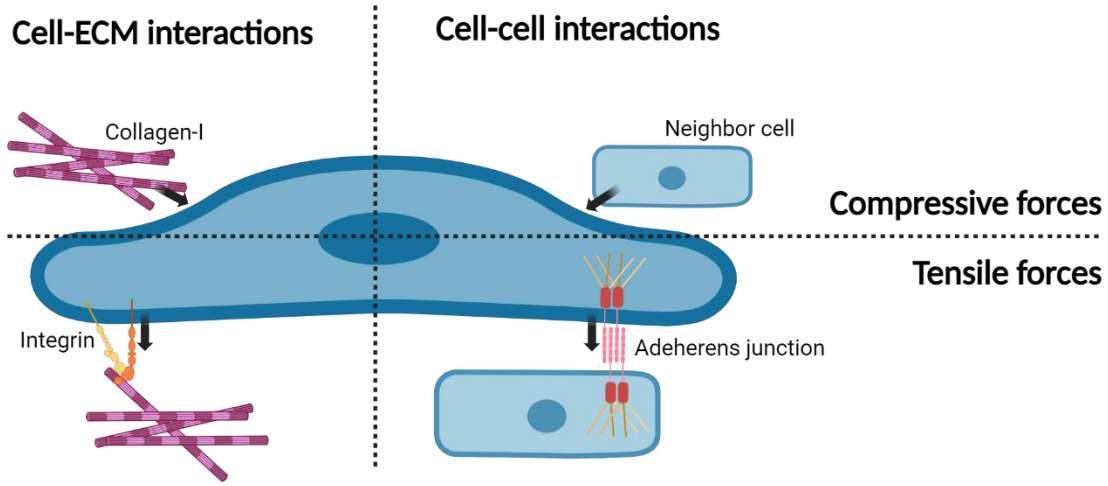

Figure 1. Types of extracellular forces that can be exerted to a cell.

There are two main types of intercellular forces: tensile and compressive (Figure 1). Tensile forces are usually originated by membrane receptor-ligand interactions, that are then transmitted to the cytoskeleton of the cell, whether this interaction comes from the ECM or a neighbor cell [12]. The ECM exerts traction forces to the cells which shape their behavior as well, affecting tissue formation (cell differentiation), development and patterning [1]. Microenvironmental forces are not only tensile, there are also extracellular compressive forces that are exerted to the cell and that usually come from compression originated by the displacement and movement of the interacting ECM or neighbor cells [12] and which do not involve any kind of receptor-ligand interactions [3].

When looking at mechanical properties of cells and their microenvironment, we should always consider that they are also governed by the fundamental laws of mechanics. This also means that, there needs to be a mechanical equilibrium in the mechanical environment of the cell. Cells balance these extracellular forces using intracellular forces: the cytoskeleton creates

compressive forces that oppose to the tensional adhesive forces exerted to cadherins by neighboring cells in cell-cell adherens junctions and in integrins in cell-ECM interactions [1,3].

The alteration of this equilibrium or of any of these mechanical interactions with the cell microenvironment could lead to tissue malformations, which can then result in various diseases including cancer. On the bright side, it also means that many of these diseases can be treated by restoring the normal mechanical equilibrium of the cell.

Furthermore, mechanics already play an important role in the treatment of several diseases at the macroscale level. An example of this could be esophageal atresia, which can be cured by restoring the normal tension distribution doing an intervention to the patient [1]. They have a special relevance in bone regeneration, since orthopedic implants are carefully designed to mimic the necessary forces to promote bone regeneration [2,13].

However, when it comes to stem cell transplantation and tissue regeneration there is still a gap in knowledge in the mechanical cues that take a part in tissue formation. However, some authors claim that the use of certain biomaterials can help address this issue and that the investigation and deeper understanding of cell mechanics could help improve cell fate after transplantation [14]. In addition, scaffolds usually have well-defined and known mechanical properties, including their elastic modulus, which can be tuned to control their behavior *in vivo* and modify their interactions with cells, including the immune response of the body. An example of this is muscle regeneration, more specifically, cardiac muscular tissue, where sarcomere organization can be controlled by altering the scaffold stiffness [2,15]. Another example would be bone transplantation, in which cell fate can be improved by altering scaffold stiffness [16-19]. The modulation of scaffold stiffness can also improve cell migration to the injury site in wound healing [20,21]. For this reason, it is clear that a further understanding of tissue mechanical forces

could lead to key insights in tissue engineering and scaffold formation [2]. This just again highlights the fact that there is a need for a tool to measure forces *in situ* to further characterize the mechanical properties of cell dense structures, tissue and organs, both *in vitro* and *in vivo* [1].

Cell forces not only play an important role in the field of tissue engineering, but also are applicable to other fields such as cancer research, since it is known that cancerous cells are stiffer than non-cancerous cells and that cancer cells signaling pathways are also controlled by mechanical cues [2,22-24]. Moreover, it is being investigated how intrinsic and extrinsic forces in the tumor microenvironment can influence the course of treatment and the resistance to therapy [25].

Despite the fact that mechanical forces play a key role in many fields like tissue regeneration and formation, wound healing and cancer, researchers in these fields have mainly focused on gene characterization, resulting in a lack of tool for characterizing cell-generated forces at the tissue level [26]. In spite of that, multiple methods to measure single-cell stiffness are available, including micropipette aspiration, microforce sensors, cell pokers, optical tweezers, and magnetic tweezers [3,10,27], but microenvironmental force measuring is still at its early stages due to the lack of technology and methods to approach 3D measurements.

A common approach to measure tissue deformation is measuring the deformation of a cell-laden gel, but it does not take into account viscosity and plasticity and does not allow force fluctuations [26]. Another approach is using a gel attached to an isometric force sensor for highly contractile cells like fibroblasts cardiac and skeletal myocytes, but it requires large tissues and is only suitable for certain cell types [26,28,29].

There are current techniques like traction force microscopy (TFM) that that attempts to tract cell mechanical properties in 2D [26,30]. In this approach a cell is placed in a well-

characterized rubber substrate that contains fluorescent particles of a much smaller size than a cell [31-33]. Then, the deformation of this substrate provoked by the force exerted to the surface by the cell is measured by monitoring the deformation of fluorescent beads embedded in the substrate (vicinities) which represent the cell environment [31,34,35]. These substrates usually have an elastic modulus in the range of 1-100 kPa and have a linear elastic behavior [32,33]. Polyacrylamide is commonly used for this approach because it is not degraded by proteases, so its mechanical properties can be assumed to remain the same over time [32,33]. Some authors have tried to translate the TFM technology to measure forces at the tissue level, and to the 3D space, but this adds a high computational complexity and 3D tissues are harder to produce and characterize [30]. Moreover, this technique is limited to *in vitro* studies, and is not suitable for *in situ* or *in vivo* measurements [3].

A similar approach is the use of micropillars, which are arrays of cantilevers or posts that can be used as a substrate, similar to TFM [26,36]. The use of cantilevers reduces the complexity of the calculations that TFM entails because it allows the use of the beam theory to resolve the deformations [26,36]. In addition, micropillar allows to measure cell-cell adhesion forces [37-39]. However, micropillars are more suitable to measure 2D forces and are not ideal for cell-dense structures [26]. Accessing a micropillar setup can also be challenging since the equipment and materials necessary to fabricate of the silicon master of the micropillar is not usually available in a standard biological laboratory [40].

Another common approach is the use of Förster Resonance Energy Transfer (FRET) sensors. This technique is based on the energy transfer of an excite-electronic-state donor fluorophore (oscillating dipole) to a neighbor acceptor fluorophore with a resonance frequency

close to the donor frequency of resonance [3]. It can be applied to measure adhesion forces in cell–cell, cell–substrate, and cell surface [41-43].

A different approach would be the use of use droplets, microparticles or microspheres as force probes. These are usually embedded in a tissue and then the mechanical properties of the microenvironment of such tissue can be extracted from different properties of the microparticle *in situ*, which can help elucidate the impact of forces in cell migration, proliferation and differentiation [3,44]. Oil droplets deform when a force greater than their interfacial tension is exerted to them, which means that these forces can be extracted from their hydrostatic pressure [3,44]. Another useful approach are ferrofluid droplets, because their magnetics properties can be used to deform them [45]and their mechanical properties can be extracted from the magnetic fields they create [46].

Our group developed polyacrylamide microparticles that can mimic cell properties [47,48]. To do so, these particles can be fabricated in a range of sizes and stiffnesses. They can also be protein-coated to mimic and better understand cell-cell and cell-ECM interactions. In our study, we evaluated different sizes, stiffnesses and coatings (uncoated, collagen-I coated, and N-cadherin coated) for microenvironmental *in situ* force measurement.

Chapter 2: Methods

Cell culture

For this experiment we cultured human adipose-derived stem cells superlot #36 (from 5 female donors, Zen-Bio, Inc.) using cell medium containing DMEM/F-12, 1% antibiotic/antimycotic (Hyclone), 10% FBS (Zen-Bio, Inc.), 1 ng/mL fibroblast growth factor, 5 ng/mL epidermal growth factor, and 0.25 ng/mL transforming growth factor-β1 (R&D Systems) at 37°C in 5% CO2. When they were 80% confluent, we trypsinized the cultured cells using 0.05% trypsin and centrifugated them for 5 minutes at 400g. We then resuspended the cells prior seeding them for 3D-cell culture.

HCMP used and protein-coating

For our experiments we used aqueous polyacrylamide hyper-compliant microparticles (HCMP) that had been previously fabricated in our lab. These were made by using a batch inverse emulsification polymerization method (and bis-acrylamide as a crosslinker) and a microdroplet generator, which allowed the fabrication of monodispersed particles in two different sizes. Two different target stiffnesses of particles were used (250Pa and 2kPa), which were achieved by modifying the acrylamide – bis-acrylamide ratios. These have an excellent biocompatibility after removing unreacted monomers, having zero effect on cell viability.

To better assess the interaction of the particles with cells, we coated them using two different proteins: collagen-I, to mimic the cell-ECM, and N-cadherin, to mimic cell-cell interactions. For the collagen-I coating, we first diluted Sulfo-SANPAH (#13414, CovaChem) and added the solution to uncoated beads. We repeatedly exposed the solution to UV light and

then washed it by using diH2o and centrifugating it at 2000g for 5 minutes. We then, left them added a collagen-I (COL-1, #08–115, Lot #2373345, Millipore) solution and stored it overnight at 4C. After this, we washed the remaining collagen-I using HCl and stored them at 4C in Phosphate Buffered Saline (PBS) until used.

For N-cadherin coating, we repeated the same process of repeatedly exposing the beads to UV light and washing them with diH2O. We then added Rabit Anti-Human IgG, Fc fragment specific and stored the solution at 4C overnight. After this, we washed the unliked N-cadherin using HBSS and added N-cadherin Protein (human N-cadherin Fc chimera Protein, R&D Systems #1388-NC) to the solution. We again waited overnight and washed the unlinked N-cadherin using PBS. We washed them for the last time with PSB and stored them in PBS at 4C until used.

We repeated both processes for both soft and stiff, small and large particles, obtaining 12 different groups of particles (Table 1).

Table 1. Particle characteristics assessed

Size	Small (15 μm target)	Large (30 μm target)	
Stiffness	Soft (250Pa target)	Stiff (2kPa target)	
Coating	Uncoated	Collagen-I	N-cadherin

We also measured the diameters of the particles used and performed a mechanical characterization of the probes. Table 2 summarizes the diameter and elastic modulus of each group of probes used in our assay.

Table 2. Particle diameter and elastic modulus

Size	Stiffness	Coating	Diameter (μm)	Elastic Modulus (Pa)
Small	Soft	Uncoated	16.3 ± 1.2	297 ± 38
		Collagen-I	17.5 ± 1.6	184 ± 23
		N-cadherin	16.3 ± 1.2	297 ± 38
	Stiff	Uncoated	15.9 ± 0.6	2063 ± 91
		Collagen-I	16.7 ± 0.9	2814 ± 389
		N-cadherin	15.9 ± 0.6	2063 ± 91
Large	Soft	Uncoated	22.6 ± 1.8	164 ± 21
		Collagen-I	22.6 ± 1.8	164 ± 21
		N-cadherin	22.6 ± 1.8	164 ± 21
	Stiff	Uncoated	34.5 ± 2.5	2317 ± 333
		Collagen-I	34.5 ± 2.5	2317 ± 333
		N-cadherin	34.5 ± 2.5	2317 ± 333

Seeding procedure

We used microtissues, more specifically, spheroids, to assess the characteristics of HCMP as force probes for microenvironmental force measurement during chondrogenesis. We created these microtissues using 2% agarose (Fisher Scientific) gels and Polydimethylsiloxane (PDMS) microtissue molds. We first combined sterile agarose and PBS then, we heated the mixture until it was homogeneous and pipetted the agarose in 96-well plates (Greiner bio-one, #655891). After this, we placed our PDMS molds on the wells that contained agarose and waited 10 minutes to let the agarose cure. Our current geometry allows us to seed 4 spheroids per well (Figure 2), which let us generate up to 368 spheroids per plate (the corner wells cannot be used due to imaging limitations). We then acclimated the gels for 24 hours using the same cell culture medium, except this time we did not use FBS (DMEM/F-12, 1% antibiotic/antimycotic (Hyclone), 1 ng/mL fibroblast growth factor, 5 ng/mL epidermal growth factor, and 0.25 ng/mL transforming growth factor-β1 (R&D Systems).

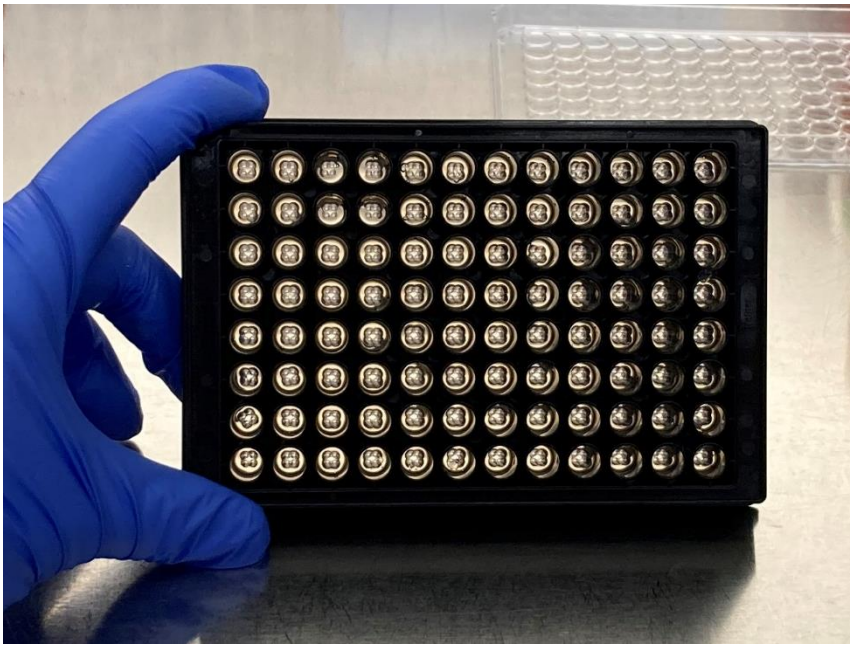

Figure 2. 96-well plate with cured 2% agarose gels before being acclimated.

After the wells were acclimated, we used a hemacytometer to count the probe type and cells to be seeded and then serially diluted to our target concentration. Our target was 1-2 particles and 5,000 cells per microwell. We combined both solutions and resuspended them until getting a homogenous solution and seeded them into our microwells (Figure 3).

We seeded all the wells of the plate except for the corner wells due to imaging limitations. We centrifugated the plate at 400g for 5 minutes to bring to solution to the bottom of our microwells. We then flooded our wells with expansion media and waited 24-48 hours after seeding to image our assembled spheroids (Figure 4).

During our earlier experiments, our goal was to take images of undeformed particles and then track them when they deformed so that we would have an accurate representation of their deformation. To do so, we first counted the particles, seeded and imaged them to get Time 0 states for all our particles. We then counted our cell suspension, using expansion medium and waited 24-48 hours before imaging again. We compared these results with the results we obtained and saw that we lost a great amount of data compared to the error introduced, so we continued our experimentation with the method described above. The results for the comparison with earlier methodology are described the Results section below. We repeated this procedure for

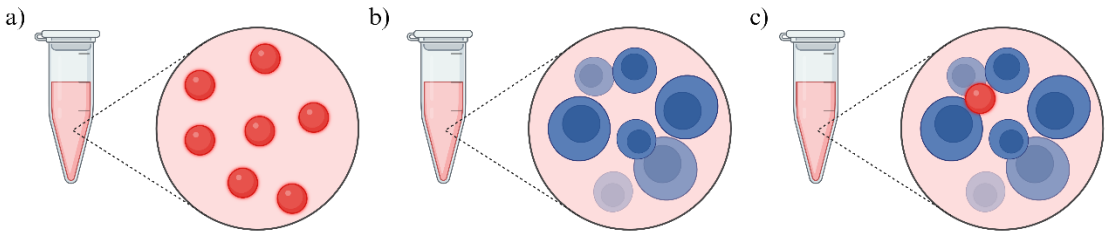

Figure 3. a) HCMP dilution at a concentration of 1,000 particles/mL, b) cell dilution at a concentration of 1,000,000 cells/mL and c) combined particle and cell dilution a t a concentration of 1,000 HCMP/mL and 1,000,000 cells/mL.

each type of particle 2-3 times to ensure that the data is consistent from run to run and that we are not getting any artificial results from a particular day.

Image acquisition

We proceeded to image our particles 24-48 hours after seeding using the Opera Phenix High-Content Screening System, which allowed us to take high-resolution 3D confocal images of our particles inside the probes. We took 3D images of the spheroids containing our probes using two channels, one with 50% 200 ms brightfield to capture the cells and another one with a 568 nm laser, for which we adjusted the exposure time and power according to the probe type (stiffer and uncoated particles are brighter). We first took 50 slices (using a 15 μm Z-slice distance) at a 10X Air magnification to detect our particles inside the spheroids and then 101 slices (using a 2 um Z-slice distance) at a 20X Water magnification (Figure 5). We used the later for our analysis, which had an XY resolution of 0.597976 um/pixel.

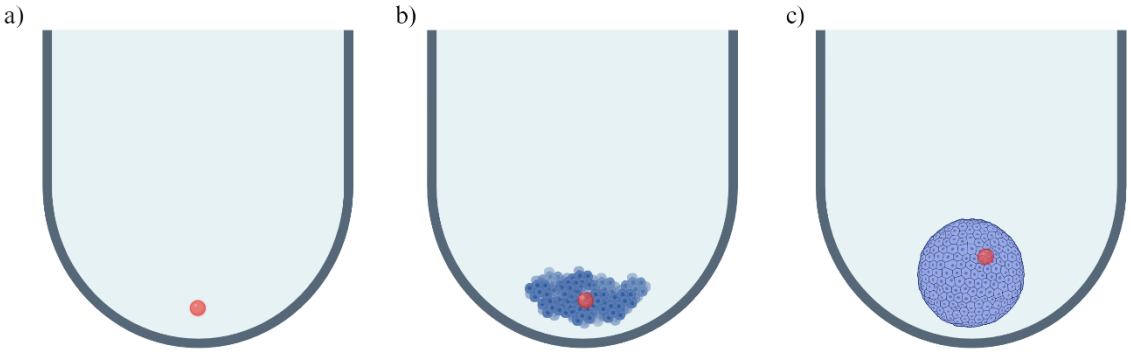

Figure 4. Microwell side view of a) seeded HCMP, b) HCMP with cells 0h after seeding, c) HCMP with cells 24-48h after seeding (during imaging)

Cytoskeletal inhibitors

We also performed an assay using cytoskeletal inhibitors to assess the return to the undeformed state of the probes after cytoskeleton disruption. We used Cytochalasin D (C823, Sigma) at a 2 μM concentration, which disrupts actin filaments; and Nocodazole (M1404, Sigma) at a 10 μM concentration, which is a microtubule disruptor. With these experiments we expected our beads to return back to their undeformed state after cytoskeletal inhibitors, since they have a mostly elastic deformation [22]. To do so, we followed the same procedure described above using large, soft, uncoated particles, since we had observed to reflect the most accurate

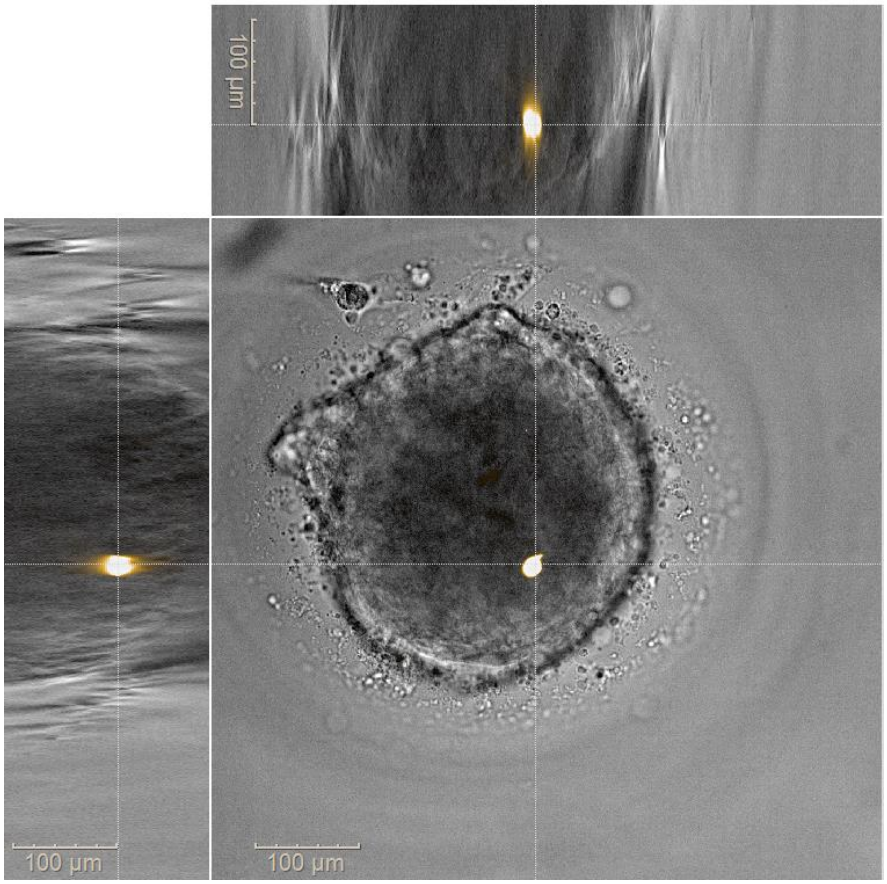

Figure 5. XYZ view of large soft uncoated particle in a spheroid at 20X Water magnification.

representation of the mechanical properties of the spheroids. After acquiring our images, we diluted Cytochalasin D and Nocodazole to the specified concentrations using the same cell medium we had been using for our experiments, changed the media of the wells for the media containing cytoskeletal inhibitors, and imaged our plate again 24 hours after treatment.

Image processing

Once we had acquired the images for each run, we binarized and cropped the 3D stacks we had acquired using a MATLAB script that processed all our images in parallel. This script also created a virtual Time 0 particle that we used as the undeformed state of our probes to extract its mechanical properties. We used the mean diameter measured for each group of particles (Table 2) to create these virtual time 0 particles based on our mean diameter for each probe type that we obtained using the methodology described above. The script extracts the XY resolution from our image embedded data and creates a perfect particle based on the input diameter. It is important to note that this resolution is around 0.5um/pixel, which limits the accuracy of the size of the virtual probe created. This script also detects whether the particles are actually inside the spheroids and then crops and binarizes the 568 nm laser channel images that only contain probes using the Otsu methodology for each stack of images. The script then individually crops each particle and placed them in a folder with the name of the particle and containing a Time 0 and Time 1 folder with the virtual Time 0 and cropped images, so that they would have the right format for the could be used in the Finite Element Analysis Mathematica program that we used to extract the mechanical properties of the probes. After running the script most of the particles that were not inside the spheroids had already been discarded. However,

due to the irregular shape of the spheroids some of them were still included in our analysis as if they were in a spheroid when they were not, so we further confirmed that the cropped particles were inside spheroids by checking each stack of the cropped particles manually, and discarding those that were not in the spheroid.

Mechanical properties extraction

To extract the mechanical properties of each probe, we used a Mathematica program developed in collaboration with the Kesari Lab from the Engineering Department here at Brown that had already been used in our lab for previous experiments [47]. This program tracks 3D cell traction by taking confocal z-stack images of different timepoints of the particles we want to study and returns the stress field, which can be displayed as a vector plot or a histogram (Figure 6). It also calculates the average pressure, elastic energy density and elastic energy of the particles. To be able to get these measurements, the first timepoint needs to be an undeformed

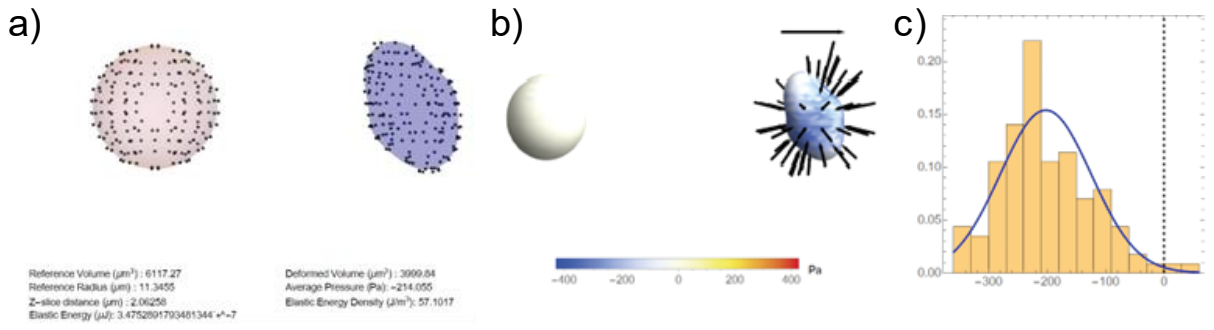

Figure 6. Example of Mathematica output of large soft uncoated HCMP (same as Figure 5). a) Undeformed and deformed 3D representation of HCMP and results of FEA, b) vectorial tractions plot (arrow size 300 Pa), c) histogram of pressure distribution

state of the particles.

For our experiments we mostly used a Parallel Processing version of such program, which returns the volume, average pressure, elastic energy density and elastic energy of the probes in their undeformed and various deformed states. The main characteristics that we will be analyzing are average pressure, which gives us an insight on whether the cells are exerting a compressive or traction pressure on the probes; and elastic energy density and elastic energy, which help us compare the magnitude of such forces. We defined the analysis parameters to be introduced in the program as showed in Figure 7, defining the elastic modulus accordingly.

The program allows the process of massive amounts of particles at the same time (as long as the probe characteristics are the same). The execution of the program creates an Excel file containing the undeformed diameter, undeformed and deformed volume, average pressure, elastic energy density and elastic energy of each particle.

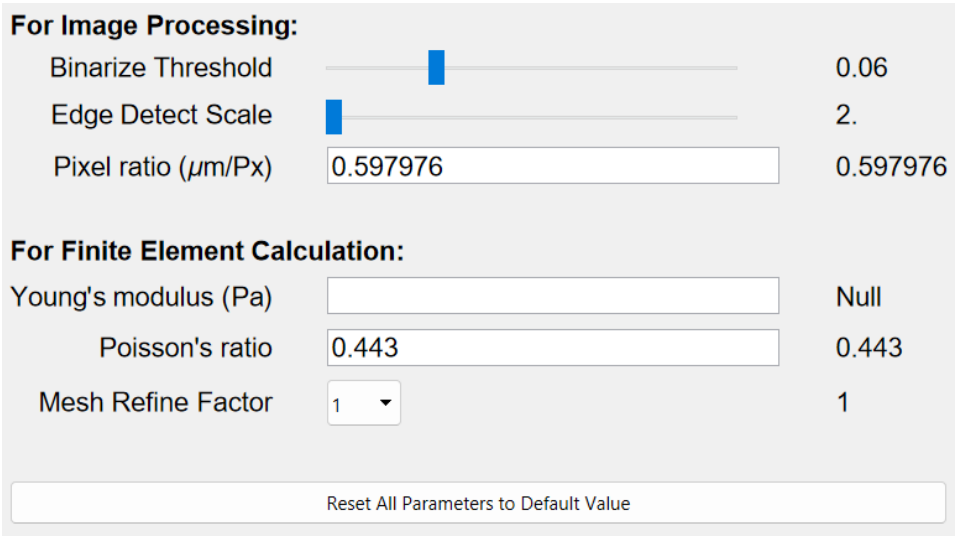

Figure 7. Parameter selection window for the Mathematica program.

Statistical analysis

We eliminated what we considered outliers (over or under mean plus minus 2.5 times standard deviation) of each run, which we assumed impossible measurements and therefore, virtual measurements due to our experiment set-up. We then plotted our data results using box and whiskers, comparing the different groups we had. To further confirm the robustness of our results, we performed one and two-way ANOVA tests as well as Dunn's tests when appropriate in our most relevant discoveries.

Real vs Virtual Time 0

To be able to understand the relevance of using a real vs virtual time 0 representation of a particle as a reference, we analyzed one soft and one stiff group of large uncoated particles and compared the results of using a real time 0 reference vs a virtual one. To do so, we changed our script so that it would discard those probes that were in a spheroid that contained more than one probe and we then matched Time 0 and Time 1 cropped files, discarding any orphans we found. We then compared the results of those same probes to the results we had obtained from our analysis and performed a one-way ANOVA between the real vs virtual time 0 particles data.

Diameter comparison

To better understand how a different Time 0 can affect our measurements, we repeated the analysis using a different Time 0 diameter: we created particles that were 1 and 2 um smaller and bigger than the original one we were using as reference. We repeated this experiment using

soft, uncoated probes, both small and large. We then analyzed the results using the same procedure as we did with the rest of our runs for each modified virtual time 0 particle, and then compared our findings to the original run (control) using a one-way ANOVA.

Chapter 3: Results

Average Pressure and Elastic Energy measurements varying probe size, stiffness and coating

We averaged the results of all the measurements obtained for the different probe types shown in Table 1. We compared the average pressure and elastic energy density for large and soft and stiff and soft uncoated particles (Figure 8) and confirmed that stiffer particles introduced more variability in both our average pressure (Figure 8a) and elastic energy density Figure 8b) measurements, and small vs large stiff particles showed statistically significant differences. Moreover, we saw that size did not have an impact on measurements within small particles but did have a statistically significant effect on stiff particles.

We also compared the effect of size and coating within soft particles for both average pressure and elastic energy (Figure 9). We observed that while uncoated probes tend to show more compressive forces, protein coated probes show more tensile forces for both small and large probes, being this more prominent in small N-cadherin particles. Nevertheless, for small

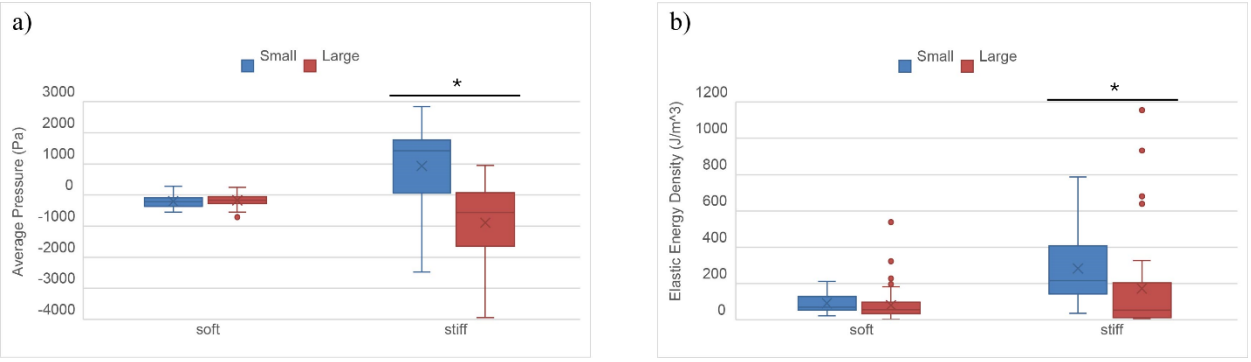

Figure 8. a) Average pressure and b) elastic energy density for small vs large and soft vs stiff uncoated probes

particles only uncoated vs N-cadherin particles showed statistically significant differences for average pressure measurements, while we observed that for large particles both uncoated vs N-cadherin and collagen-I vs N-cadherin particles showed statistically significant differences in average pressure. When looking at the elastic energy measurements, we observed that large particles presented similar elastic energy measurements between all coatings, whereas small N-cadherin particles showed greater elastic energy measurements than uncoated and collagen-I coated particles. These findings were confirmed by the statistical analysis, which showed statistically significant differences in elastic energy for uncoated vs N-cadherin and collagen-I vs N-cadherin for small particles, and did not show any significant differences between the coatings for large particles.

Use of a virtual undeformed state assessment

To confirm that using a virtual undeformed Time 0 particle was plausible, we compared the results when using virtual vs real Time 0 data. When looking at soft probes, we found that even

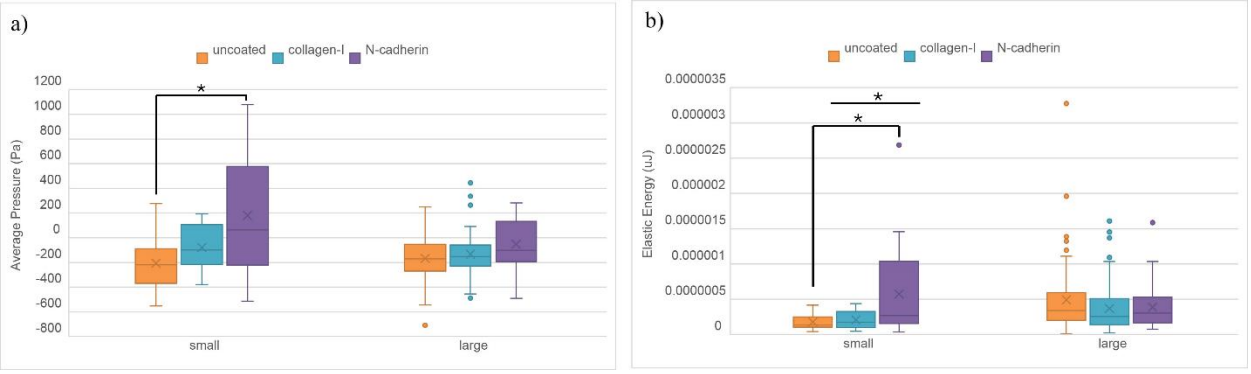

Figure 9. a) Average pressure and b) elastic energy density for uncoated vs collagen-I vs N-cadherin coated small and large soft probes

though the amount of data collected was considerably lower than when using a virtual Time 0 (17 vs 32 data points), the measurements were relatively similar (Figure 10a and Figure 10b). This finding was further confirmed by the statistical analysis performed, which revealed that

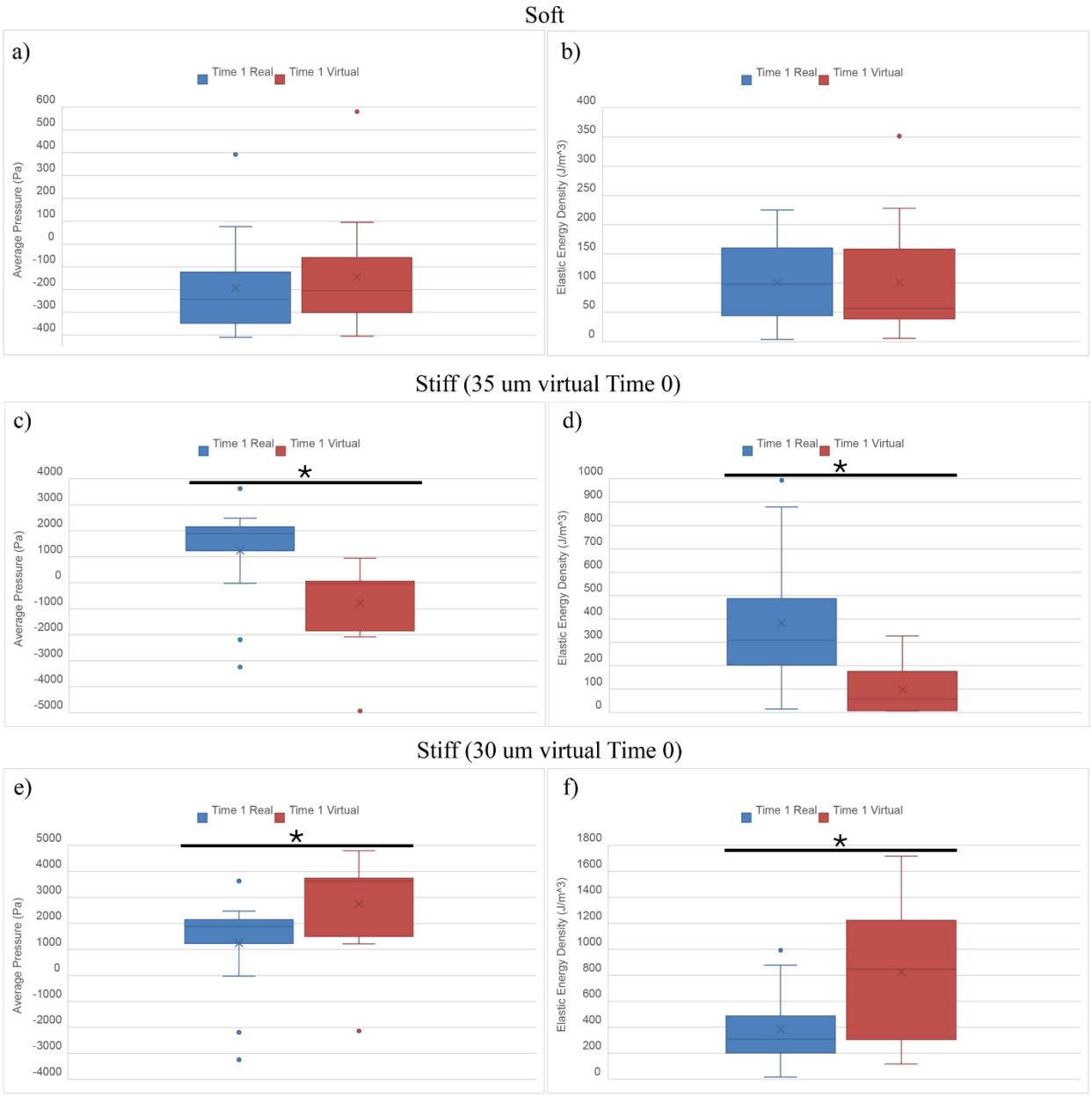

Figure 10. Comparison using a real vs virtual undeformed state of average pressure and elastic energy density of large soft, a) and b) respectively, and stiff using a 35 um, c) and d) 30 um virtual Time 0 respectively, uncoated HCMP.

there is no statistically significant difference between the average pressure (P = 0,480) or elastic energy density (P = 0.744) measurements in both groups for soft probes.

We repeated this approach using large stiff probes and, although the data loss was similar compared to soft probes (15 vs 42 data points), the measurements were significantly different for both average pressure and elastic energy density (Figure 10c and Figure 10d). These findings were further confirmed by the statistical analysis, which revealed significant differences for both

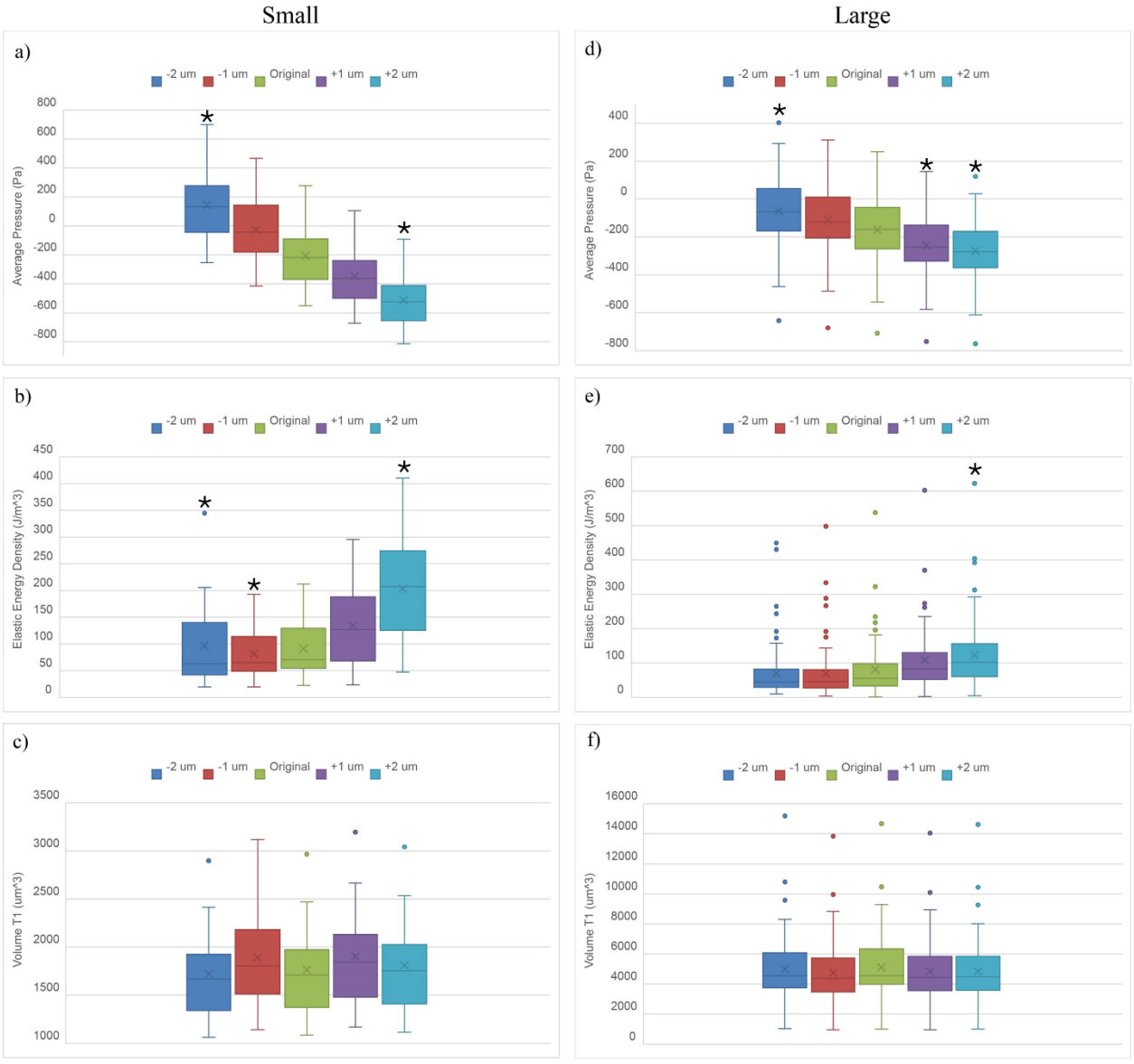

Figure 11. Comparison of average pressure, elastic energy density and time 1 volume modifying the time 0 diameter for small a), b), and c) and large d), e) and f) probes respectively.

average pressure (P = 0.001) and elastic energy density (P = 0.002). We observed that the 35 μm virtual time 0 was considerably larger than the real time 0 diameters. For this reason, we repeated the analysis using a 30 μm virtual time 0 (Figure 10e and Figure 10f), which again revealed significant differences for both average pressure (P = 0.010) and elastic energy density (P = 0.015).

We also wanted to evaluate the error we were introducing by employing this approach. For this reason, we compared the results of average pressure and elastic energy density obtained when incrementing or decreasing the virtual Time 0 particle size by 1 and 2 μm (Figure 11a, b, d, e). When looking at the diameter comparisons we performed, it becomes clear that the average pressure shifts when increasing or decreasing the virtual time 0 diameter (Figure 11a, b, d, e). If

Table 3. Statistical analysis for diameter comparison

		Average Pressure	**Elastic Energy**
Small	**-2 um**	Yes (P<0.001)	Yes (P = 0.013)
	-1 um	No (P = 0.135)	Yes (P = 0.001)
	+1 um	No (P = 0.285)	No (P = 0.148)
	+2 um	Yes (P<0.001)	Yes (P<0.001)
Large	**-2 um**	Yes (P = 0.002)	No (P = 1.000)
	-1 um	No (P = 0.225)	No (P = 0.110)
	+1 um	Yes (P = 0.005)	No (P = 0.196)
	+2 um	Yes (P<0.001)	Yes (P = 0.001)

we look at the result of the statistical analysis performed (Table 3), it shows statistical differences for the probes closer to the original diameter and less statistically significant differences for large probes than it does for smaller probes, as could be expected, since smaller probes introduce a greater error. We also compared the difference between the resolved Time 1 volume for each of the undeformed sizes (Figure 11c, f), since the z-slice distance is extracted from the undeformed state, and although the are some differences, they all remained similar to the original undeformed state size.

Cytoskeletal modulators effect on mechanical properties measurements

Our cytoskeletal inhibitor assay showed an average pressure and elastic energy density closer to 0 for spheroids treated with Cytochalasin D (Figure 12). In contrast, spheroids treated with Nocodazole show similar results to untreated probes for both the average pressure and elastic energy density. These results were further confirmed by the statistical analysis, which showed a statistically significant difference between the control and cytochalasin D treated

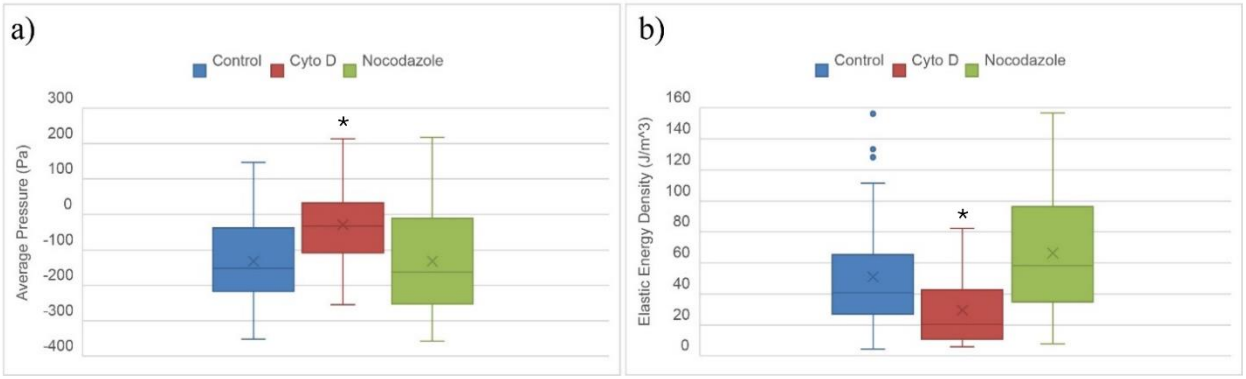

Figure 12. a) Average pressure and b) elastic energy density for the control group and using cytoskeletal inhibitors (cytochalasin D and Nocodazole) for large, soft, uncoated probes.

spheroids but did not show a statistically significant difference between the control and Nocodazole treated spheroids.

Chapter 4: Discussion and Conclusions

The data collected for this study overall suggests that the method proposed can be used to measure forces in microenvironments *in situ*. The use of different protein coatings allows the measurement of cell-cell interactions and cell-ECM interactions. Our data suggests that neighbor cells can both exert compressive forces (uncoated) and tensile forces through cell adhesions (N-cadherin)[3,12]. In addition, cell-ECM interactions can also exert both compressive and tensile forces via relative movement and protein binding interactions respectively. Both confirm previous findings, since protein-bound cell-ECM interactions and cell-cell adhesion have been observed to transmit tensile forces [2,12]. Nonetheless, N-cadherin coated HCMP showed more greater forces, which were more pronounced in small probes because, as previously stated, show more sparse measurements because the error introduced through the relative size of the probe to the resolution is greater. This could be explained by our set up or by the fact that there was a greater data loss when using N-cadherin particles. It is also important to mention that all coating showed measured forces within the same force range, since the elastic energy measurements for all coatings were found to be similar (Figure 9b).

When looking at uncoated probes (Figure 8), we confirmed our previous findings: stiffer probes show a more variability in measurements, while softer probes give a more accurate representation [47]. This could be explained by the fact that a small deformation in a stiffer probe results in a greater stress, which will then contribute to a greater average pressure and elastic energy density. When looking at the size of the probe (Figure 8), we do not observe a significant effect on the on the measured average pressure in soft probes. Despite having hypothesized that different sizes could measure different force ranges, our findings suggest that rather than

different force ranges, the use of different sizes impacts measurements resolution. This translates into the fact that the resolution of the obtained measurements is limited by the resolution that the set up offers. Moreover, small probes can also introduce a lack of resolution in measurements since their size is more similar to cell sizes. If we look at stiff probes, we observe that smaller probes result in more positive measurements (Figure 8). We found similar results for collagen-I and N-cadherin coated probes. These findings were further confirmed by the statistical analysis, which did not show significant differences in size for soft probes. However, it did show significant differences between sizes within stiff probes and between stiffnesses for both sizes, probably due to the lack of resolution added when using stiffer probes.

In addition, we validated our study by performing a cytoskeletal inhibitor assay. The disruption of the actin filaments in the spheroids restored the HCMP initial state as observed in previous work [44,47], while microtubule disruption did not have an impact on measurements. This could be explained by the fact that the use of Nocodazole can increase cell stiffness [49], which would not let the force probes restore its original shape.

We verified that the use of a virtual Time 0 when using soft probes is feasible by virtually creating an undeformed state of the particle. This statement mostly relies on the monodispersity of the particles used in the experiment. However, we observed significant differences when employing stiff probes, which could be explained by the variability introduced by stiffer probes. We further analyzed the error introduced by comparing our data to the measurements obtained when incrementing and reducing the virtual Time 0 diameter by 1 and 2 μm. The shift in average pressure and elastic energy measurements once again highlights the importance of the monodispersity of the particles used in our experiments. It also elucidates the error we might be introducing into our results and helps assess whether a real Time 0 measurement should be

employed when using this technique. Moreover, smaller probes show a bigger shift in measurements as anticipated (Figure 11), since we need to keep in mind that we have a resolution of ~0.6 μm/pixel in the XY axes and Z-slice distance of 2 μm.

Nonetheless, there are certain limitations in our study that are important to consider. We found inconsistencies in terms of number of data results when caring out experiments. Despite using the same setup, some runs were considered successful (with > 100 data points) whereas others had none or very few good datapoints. We hypothesize that this is due to the lack of control we have when it comes to the seeding procedure: we need 1-2 probes per microwell that are achieved by seeding at a low concentration, which would lead to some cases where all the probes would go to a certain microwell our too many or not enough would make it to the well. Moreover, the probes need to end up inside the spheroid, which sometimes could be hard to achieve as well. It is also important to acknowledge the fact that we were assuming a virtual Time 0 based on the probe size and that this is going to introduce a certain error to our measurements as we can see in the diameter comparison section above. This error will be highly dependent on the resolution of our images and the standard deviation of the diameter of the probes employed.

Future lines of this study could include the use of HCMP as force probes to acquire quantitative data for *in situ* microenvironmental force measurements. These could include both stem cell condensation, proliferation or even differentiation. Moreover, the impact of image resolution and probe size on measurements could be explored, by using higher resolution images and HCMP considerably larger than the ones employed. Another line to be considered could be the use of stiffer cells and the impact of relative elastic modulus compared to cell modulus. Finally, the impact of cytoskeletal modulators such as Blebbistatin (myosin II inhibitor) or taxol

(microtubule stabilizer) could be further studied, as well as the impact of their recovery from Nocodazole.

References

1. Mammoto T, Ingber DE. Mechanical control of tissue and organ development. *Development*. 2010-05-01 2010;137(9):1407-1420. doi:10.1242/dev.024166
2. Vining KH, Mooney DJ. Mechanical forces direct stem cell behaviour in development and regeneration. *Nature Reviews Molecular Cell Biology*. 2017-12-01 2017;18(12):728-742. doi:10.1038/nrm.2017.108
3. Sutlive J, Xiu H, Chen Y, et al. Generation, Transmission, and Regulation of Mechanical Forces in Embryonic Morphogenesis. *Small*. 2022-02-01 2022;18(6):2103466. doi:10.1002/smll.202103466
4. Spedden E, White D, James, Naumova N, Elena, Kaplan L, David, Staii C. Elasticity Maps of Living Neurons Measured by Combined Fluorescence and Atomic Force Microscopy. *Biophysical Journal*. 2012-09-01 2012;103(5):868-877. doi:10.1016/j.bpj.2012.08.005
5. Solon J, Kaya-Çopur A, Colombelli J, Brunner D. Pulsed Forces Timed by a Ratchet-like Mechanism Drive Directed Tissue Movement during Dorsal Closure. *Cell*. 2009-06-01 2009;137(7):1331-1342. doi:10.1016/j.cell.2009.03.050
6. Watanabe K, Ueno M, Kamiya D, et al. A ROCK inhibitor permits survival of dissociated human embryonic stem cells. *Nature Biotechnology*. 2007-06-01 2007;25(6):681-686. doi:10.1038/nbt1310
7. Jin H, Xing X, Zhao H, et al. Detection of erythrocytes influenced by aging and type 2 diabetes using atomic force microscope. *Biochem Biophys Res Commun*. Jan 22 2010;391(4):1698-702. doi:10.1016/j.bbrc.2009.12.133
8. Alcaraz J, Buscemi L, Grabulosa M, et al. Microrheology of Human Lung Epithelial Cells Measured by Atomic Force Microscopy. *Biophysical Journal*. 2003-03-01 2003;84(3):2071-2079. doi:10.1016/s0006-3495(03)75014-0
9. Lekka M, Gil D, Pogoda K, et al. Cancer cell detection in tissue sections using AFM. *Arch Biochem Biophys*. Feb 15 2012;518(2):151-6. doi:10.1016/j.abb.2011.12.013
10. Jung W, Li J, Chaudhuri O, Kim T. Nonlinear Elastic and Inelastic Properties of Cells. *Journal of Biomechanical Engineering*. 2020-10-01 2020;142(10)doi:10.1115/1.4046863
11. Maurer M, Lammerding J. The Driving Force: Nuclear Mechanotransduction in Cellular Function, Fate, and Disease. *Annual Review of Biomedical Engineering*. 2019-06-04 2019;21(1):443-468. doi:10.1146/annurev-bioeng-060418-052139
12. Chen Y, Li Z, Ju LA. Tensile and compressive force regulation on cell mechanosensing. *Biophys Rev*. Jun 2019;11(3):311-318. doi:10.1007/s12551-019-00536-z
13. Kessler P, Neukam FW, Wiltfang J. Effects of distraction forces and frequency of distraction on bony regeneration. *Br J Oral Maxillofac Surg*. Oct 2005;43(5):392-8. doi:10.1016/j.bjoms.2004.10.015
14. Mao AS, Shin J-W, Utech S, et al. Deterministic encapsulation of single cells in thin tunable microgels for niche modelling and therapeutic delivery. *Nature Materials*. 2017-02-01 2017;16(2):236-243. doi:10.1038/nmat4781
15. Lee S, Serpooshan V, Tong X, et al. Contractile force generation by 3D hiPSC-derived cardiac tissues is enhanced by rapid establishment of cellular interconnection in matrix with muscle-mimicking stiffness. *Biomaterials*. 2017-07-01 2017;131:111-120. doi:10.1016/j.biomaterials.2017.03.039

16. Liu M, Zeng X, Ma C, et al. Injectable hydrogels for cartilage and bone tissue engineering. *Bone Research*. 2017-05-30 2017;5(1):17014. doi:10.1038/boneres.2017.14
17. Cilla M, Checa S, Duda GN. Strain shielding inspired re-design of proximal femoral stems for total hip arthroplasty. *Journal of Orthopaedic Research*. 2017-11-01 2017;35(11):2534-2544. doi:10.1002/jor.23540
18. Olivares-Navarrete R, Lee EM, Smith K, et al. Substrate Stiffness Controls Osteoblastic and Chondrocytic Differentiation of Mesenchymal Stem Cells without Exogenous Stimuli. *PLOS ONE*. 2017-01-17 2017;12(1):e0170312. doi:10.1371/journal.pone.0170312
19. Darnell M, Young S, Gu L, et al. Substrate Stress-Relaxation Regulates Scaffold Remodeling and Bone Formation In Vivo. *Advanced Healthcare Materials*. 2017-01-01 2017;6(1):1601185. doi:10.1002/adhm.201601185
20. Yang H, Nguyen KT, Leong DT, Tan NS, Tay CY. Soft Material Approach to Induce Oxidative Stress in Mesenchymal Stem Cells for Functional Tissue Repair. *ACS Appl Mater Interfaces*. Oct 12 2016;8(40):26591-26599. doi:10.1021/acsami.6b09222
21. Griffin DR, Weaver WM, Scumpia PO, Di Carlo D, Segura T. Accelerated wound healing by injectable microporous gel scaffolds assembled from annealed building blocks. *Nature Materials*. 2015-07-01 2015;14(7):737-744. doi:10.1038/nmat4294
22. Zhang S, Grifno G, Passaro R, et al. Intravital measurements of solid stresses in tumours reveal length-scale and microenvironmentally dependent force transmission. *Nature Biomedical Engineering*. 2023-08-28 2023;7(11):1473-1492. doi:10.1038/s41551-023-01080-8
23. Chaudhuri O, Koshy ST, Branco Da Cunha C, et al. Extracellular matrix stiffness and composition jointly regulate the induction of malignant phenotypes in mammary epithelium. *Nature Materials*. 2014-10-01 2014;13(10):970-978. doi:10.1038/nmat4009
24. Saxena M, Liu S, Yang B, et al. EGFR and HER2 activate rigidity sensing only on rigid matrices. *Nature Materials*. 2017-07-01 2017;16(7):775-781. doi:10.1038/nmat4893
25. Shin J-W, Mooney DJ. Extracellular matrix stiffness causes systematic variations in proliferation and chemosensitivity in myeloid leukemias. *Proceedings of the National Academy of Sciences*. 2016-10-25 2016;113(43):12126-12131. doi:10.1073/pnas.1611338113
26. Polacheck WJ, Chen CS. Measuring cell-generated forces: a guide to the available tools. *Nature Methods*. 2016-05-01 2016;13(5):415-423. doi:10.1038/nmeth.3834
27. Lulevich V, Shih Y-P, Lo SH, Liu G-Y. Cell Tracing Dyes Significantly Change Single Cell Mechanics. *The Journal of Physical Chemistry B*. 2009-05-07 2009;113(18):6511-6519. doi:10.1021/jp8103358
28. Delvoye P, Wiliquet P, Leveque JL, Nusgens BV, Lapiere CM. Measurement of mechanical forces generated by skin fibroblasts embedded in a three-dimensional collagen gel. *J Invest Dermatol*. Nov 1991;97(5):898-902. doi:10.1111/1523-1747.ep12491651
29. Dennis RG, Kosnik PE, 2nd. Excitability and isometric contractile properties of mammalian skeletal muscle constructs engineered in vitro. *In Vitro Cell Dev Biol Anim*. May 2000;36(5):327-35. doi:10.1290/1071-2690(2000)036<0327:EAICPO>2.0.CO;2
30. Song D, Dong L, Gupta M, et al. Recovery of Tractions Exerted by Single Cells in Three-Dimensional Nonlinear Matrices. *J Biomech Eng*. Aug 1 2020;142(8)doi:10.1115/1.4046974
31. Harris AK, Stopak D, Wild P. Fibroblast traction as a mechanism for collagen morphogenesis. *Nature*. 1981-03-01 1981;290(5803):249-251. doi:10.1038/290249a0

32. Oliver T, Jacobson K, Dembo M. Design and use of substrata to measure traction forces exerted by cultured cells. *Methods Enzymol*. 1998;298:497-521. doi:10.1016/s0076-6879(98)98042-9
33. Beningo KA, Wang YL. Flexible substrata for the detection of cellular traction forces. *Trends Cell Biol*. Feb 2002;12(2):79-84. doi:10.1016/s0962-8924(01)02205-x
34. Patil LS, Varner VD. Toward Measuring the Mechanical Stresses Exerted by Branching Embryonic Airway Epithelial Explants in 3D Matrices of Matrigel. *Annals of Biomedical Engineering*. 2022-09-01 2022;50(9):1143-1157. doi:10.1007/s10439-022-02989-y
35. Legant WR, Miller JS, Blakely BL, Cohen DM, Genin GM, Chen CS. Measurement of mechanical tractions exerted by cells in three-dimensional matrices. *Nature Methods*. 2010-12-01 2010;7(12):969-971. doi:10.1038/nmeth.1531
36. Tan JL, Tien J, Pirone DM, Gray DS, Bhadriraju K, Chen CS. Cells lying on a bed of microneedles: An approach to isolate mechanical force. *Proceedings of the National Academy of Sciences*. 2003-02-18 2003;100(4):1484-1489. doi:10.1073/pnas.0235407100
37. Ganz A, Lambert M, Saez A, et al. Traction forces exerted through N-cadherin contacts. *Biology of the Cell*. 2006-12-01 2006;98(12):721-730. doi:10.1042/bc20060039
38. Liu Z, Tan JL, Cohen DM, et al. Mechanical tugging force regulates the size of cell–cell junctions. *Proceedings of the National Academy of Sciences*. 2010-06-01 2010;107(22):9944-9949. doi:10.1073/pnas.0914547107
39. Maruthamuthu V, Sabass B, Schwarz US, Gardel ML. Cell-ECM traction force modulates endogenous tension at cell–cell contacts. *Proceedings of the National Academy of Sciences*. 2011-03-22 2011;108(12):4708-4713. doi:10.1073/pnas.1011123108
40. Yang MT, Fu J, Wang Y-K, Desai RA, Chen CS. Assaying stem cell mechanobiology on microfabricated elastomeric substrates with geometrically modulated rigidity. *Nature Protocols*. 2011-02-01 2011;6(2):187-213. doi:10.1038/nprot.2010.189
41. Borghi N, Sorokina M, Shcherbakova OG, et al. E-cadherin is under constitutive actomyosin-generated tension that is increased at cell–cell contacts upon externally applied stretch. *Proceedings of the National Academy of Sciences*. 2012-07-31 2012;109(31):12568-12573. doi:10.1073/pnas.1204390109
42. Grashoff C, Hoffman BD, Brenner MD, et al. Measuring mechanical tension across vinculin reveals regulation of focal adhesion dynamics. *Nature*. 2010-07-01 2010;466(7303):263-266. doi:10.1038/nature09198
43. Stabley DR, Jurchenko C, Marshall SS, Salaita KS. Visualizing mechanical tension across membrane receptors with a fluorescent sensor. *Nature Methods*. 2012-01-01 2012;9(1):64-67. doi:10.1038/nmeth.1747
44. Campàs O, Mammoto T, Hasso S, et al. Quantifying cell-generated mechanical forces within living embryonic tissues. *Nature Methods*. 2014-02-01 2014;11(2):183-189. doi:10.1038/nmeth.2761
45. Doubrovinski K, Swan M, Polyakov O, Wieschaus EF. Measurement of cortical elasticity in Drosophila melanogaster embryos using ferrofluids. *Proc Natl Acad Sci U S A*. Jan 31 2017;114(5):1051-1056. doi:10.1073/pnas.1616659114
46. Serwane F, Mongera A, Rowghanian P, et al. In vivo quantification of spatially varying mechanical properties in developing tissues. *Nature Methods*. 2017-02-01 2017;14(2):181-186. doi:10.1038/nmeth.4101

47. Gutierrez RA, Fang W, Kesari H, Darling EM. Force sensors for measuring microenvironmental forces during mesenchymal condensation. *Biomaterials*. Mar 2021;270:120684. doi:10.1016/j.biomaterials.2021.120684
48. Labriola NR, Mathiowitz E, Darling EM. Fabricating polyacrylamide microbeads by inverse emulsification to mimic the size and elasticity of living cells. *Biomaterials Science*. 2017-01-01 2017;5(1):41-45. doi:10.1039/c6bm00692b
49. Sen S, Kumar S. Cell–Matrix De-Adhesion Dynamics Reflect Contractile Mechanics. *Cellular and Molecular Bioengineering*. 2009-06-01 2009;2(2):218-230. doi:10.1007/s12195-009-0057-7

Appendix A

Too soft probes result in in complex geometries that cannot be processed by our program

We compared 86 Pa and both small and large soft particle measurements (Supplemental Figure 1), since we encountered that 86 Pa were too soft to use: some of the geometries could not be resolved and resulted in negative or imaginary values for the volumes (~1 for every 20 good datapoints). We performed a 2-way ANOVA and it showed a statistically significant difference between the means of the average pressure of soft vs 86 Pa overall and within collagen-I and N-cadherin coatings but not with uncoated probes. Within 86 Pa probes, it again only shows a significant difference of the means of average pressure between uncoated vs N-cadherin coated particles.

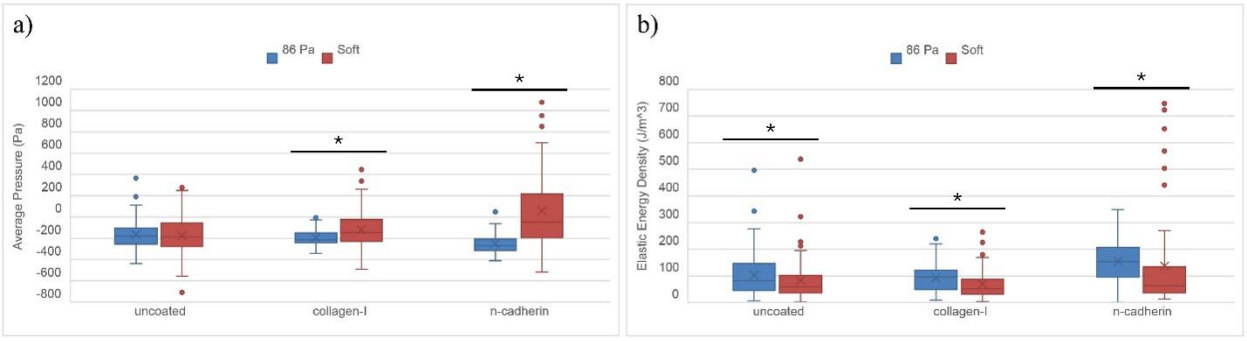

Supplemental Figure 1. 86 Pa vs Soft probes for uncoated, collagen-I coated and N-cadherin coatings a) average pressure and b) elastic energy density.